Accepted Manuscript

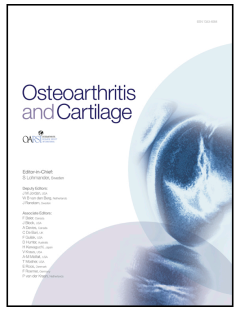

Relationships between *in vivo* dynamic knee joint loading, static alignment and tibial subchondral bone microarchitecture in end-stage knee osteoarthritis

Bryant C. Roberts, Lucian B. Solomon, Graham Mercer, Karen J. Reynolds, Dominic Thewlis, Egon Perilli

PII: S1063-4584(18)30064-5

DOI: 10.1016/j.joca.2018.01.014

Reference: YJOCA 4152

To appear in: *Osteoarthritis and Cartilage*

Received Date: 11 November 2016

Revised Date: 11 January 2018

Accepted Date: 18 January 2018

Relationships between *in vivo* dynamic knee joint loading, static alignment and tibial subchondral bone microarchitecture in end-stage knee osteoarthritis

Bryant C Roberts[a], Lucian B Solomon[b,c], Graham Mercer[d], Karen J Reynolds[a], Dominic Thewlis[b,c,e*]
Egon Perilli[a*]

*Joint senior authors

[a]The Medical Device Research Institute, College of Science and Engineering, Flinders University, Adelaide, South Australia, Australia

[b]Department of Orthopaedics and Trauma, Royal Adelaide Hospital, Adelaide, South Australia, Australia

[c]Centre for Orthopaedic and Trauma Research, The University of Adelaide, Adelaide, South Australia, Australia

[d]Department of Orthopaedic Surgery, Repatriation General Hospital, Daws Park, South Australia, Australia

[e]Alliance for Research in Exercise, Nutrition and Activity, Sansom Institute for Health Research, University of South Australia, Adelaide, South Australia, Australia

Corresponding author:

Egon Perilli, The Medical Device Research Institute, College of Science and Engineering, Flinders University, GPO Box 2100, Adelaide, South Australia, 5001, Australia. Ph: +61 8 8201 3586. E-mail: egon.perilli@flinders.edu.au

Running title:

Knee joint loading and bone microarchitecture

Abstract

Objective: To study, in end-stage knee osteoarthritis (OA) patients, relationships between indices of *in vivo* dynamic knee joint loads obtained pre-operatively using gait analysis, static knee alignment, and the subchondral trabecular bone (STB) microarchitecture of their excised tibial plateau quantified with 3D micro-CT.

Design: Twenty-five knee OA patients scheduled for total knee arthroplasty underwent pre-operative gait analysis. Mechanical axis deviation (MAD) was determined radiographically. Following surgery, excised tibial plateaus were micro-CT-scanned and STB microarchitecture analysed in four subregions (anteromedial, posteromedial, anterolateral, posterolateral). Regional differences in STB microarchitecture and relationships between joint loading and microarchitecture were examined.

Results: STB microarchitecture differed among subregions ($p<0.001$), anteromedially exhibiting highest bone volume fraction (BV/TV) and lowest structure model index (SMI). Anteromedial BV/TV and SMI correlated strongest with peak external rotation moments (ERM; $r=-0.74$, $r=0.67$, $p<0.01$), despite ERM being the lowest (by factor of 10) of the moments considered, with majority of ERM measures below accuracy thresholds; medial-to-lateral BV/TV ratios correlated with ERM, MAD, and knee adduction (KAM) and internal rotation moments ($|r|$-range: 0.54-0.74). When controlling for walking speed, KAM and MAD, the ERM explained additional 11-30% of the variations in anteromedial BV/TV and medial-to-lateral BV/TV ratio ($R^2=0.59$, $R^2=0.69$, $p<0.01$).

Conclusions: This preliminary study suggests significant associations between tibial plateau STB microarchitecture and knee joint loading indices in end-stage knee OA patients. Particularly, anteromedial BV/TV correlates strongest with ERM, whereas medial-to-lateral BV/TV ratio correlates strongest with indicators of medial-to-lateral joint loading (MAD, KAM) and rotational moments. However, associations with ERM should be interpreted with caution.

Keywords

knee osteoarthritis, gait biomechanics, micro-CT, subchondral trabecular bone, bone microarchitecture

1. Introduction

Knee osteoarthritis (OA) is a debilitating disease affecting all tissues within the joint, including bone. The subchondral bone is a mechanical shock absorber, protecting the overlying articular cartilage from excessive joint loads[1]. The compromised integrity of subchondral bone plays an important role in the onset and progression of the disease[1,2]. In prospective studies, abnormal joint biomechanics that is common with knee OA[3,4], has been associated with rate of radiographic disease progression[5,6], while in cross-sectional studies, it has been linked with variations to joint structures (e.g. presence of cartilage defects[7], bone marrow lesions[8], variations in subchondral bone area[7,9] and cartilage thickness[10]).

Abnormal *in vivo* joint loads, indicated by frontal plane loading indices, such as knee adduction moment (KAM) measured during gait and static knee alignment from radiographs, have been associated with local variations in proximal tibia bone mineral density (BMD) and mineral content (BMC), measured by dual X-ray absorptiometry (DXA)[11-13]. DXA, however, is a two-dimensional technique which has limited spatial resolution and cannot differentiate between cortical and trabecular bone, or among different subregions within the same condyle. Furthermore, it cannot quantify bone microarchitecture, which has been shown to vary within the OA proximal tibia[14-16].

To understand the degeneration of subchondral bone in OA, it is necessary to study its microarchitecture. However, previous studies examining subchondral bone microarchitecture in humans were restricted to thin histological slices or excised bone cores[14,15]. Nowadays, X-ray micro-computed tomography (micro-CT) allows three-dimensional (3D) structural characterization of entire bone segments including the tibial plateau, non-destructively and at high resolution[16-18]. Moreover, to the best of our knowledge, those studies exploring the bone microarchitecture, did not examine gait or *in vivo* joint biomechanics data from the same patients, to investigate possible relationships between these measures. Thus, the associations between knee joint biomechanics (including the full 3D knee moments, which differ from normal in OA[3,4]) and tibial subchondral trabecular bone (STB) microarchitecture in OA, in the same patient, remain to be investigated. Through a better understanding of how joint loading is related to local variations in subchondral bone micro-architecture in knee OA, it may be possible to better describe the role of both factors in the disease.

This study explores, in end-stage OA patients undergoing total knee arthroplasty (TKA), relationships between indices of *in vivo* dynamic knee joint loads obtained pre-operatively using 3D gait analysis (full 3D knee moments, tibiofemoral joint reaction forces), static knee alignment (mechanical axis deviation, medial proximal tibial angle) and regional proximal tibia subchondral bone microarchitecture of their excised knees quantified with 3D micro-CT. The objective was to determine which biomechanical factors described the greatest variation in subregional subchondral trabecular bone microarchitecture and distribution of the bone across the tibia plateau. We hypothesised that the frontal plane loading indices (static alignment, peak adduction moments and impulse), indicators of medial tibial compartment loading[19] and medial-to-lateral distribution of load[20], would be factors most strongly associated with the medial condyle STB microarchitecture and medial-to-lateral distribution of bone in the tibial plateau.

2. Methods

2.1 Participants

Twenty-five (n=25) adult patients with end-stage knee OA, scheduled for TKA, were recruited from the orthopaedics departments at the Royal Adelaide Hospital, Repatriation General Hospital and Burnside War Memorial Hospital in Adelaide, Australia (Table 1). In all patients indication for surgery was painful and symptomatic knee OA, and unsatisfactory response to non-invasive treatments. This criteria established our operational definition of end-stage knee OA. The radiographic (Kellgren-Lawrence) grade of the examined joints ranged from 2 (mild) to 4 (severe; Table 2). Patients were excluded from this study if: they were unable to walk unaided for 10 m; had a history of inflammatory arthritis; had neurological disorders that would affect walking; had severe cardiovascular or pulmonary disease; had isolated patellofemoral knee OA; or were unable to understand English. This study received ethics approval from the Southern Adelaide Clinical and

Royal Adelaide Hospital Human Research Ethics Committees. All patients provided written informed consent prior to their involvement.

2.2 Gait analysis

Patients underwent pre-operative gait analysis within one week prior to surgery. Three successful walking trials were collected with the patient walking, without footwear, at self-selected speed along a 10-m walkway. 3D kinematics and ground reaction force data were collected using 12 VICON MX-F20 cameras (Vicon Metrics, Oxford, UK) and four floor-embedded force platforms (2 × 9281B, Kistler Instrument Corporation, Switzerland; 2 × AMTI BP400600, Advanced Mechanical Technology Inc., USA) at 100 and 400 Hz, respectively. A set of 40 retro-reflective lower-limb markers were placed on the subject's pelvis and lower limbs. Markers were placed over palpable anatomical landmarks to define the joints of the lower limbs, and rigid clusters of four non-collinear markers were attached to the thighs and shanks[21]. Marker trajectories and ground reaction forces were low-pass filtered, using a zero-lag 4^{th} order Butterworth filter with cut-off frequency of 6 and 25 Hz, respectively[22]. The pose of the body segments was reconstructed using global optimisation[23] . The kinematic model (details in Thewlis et al.[24]) consisted of a pelvis, two thighs, two shanks and two feet connected by six joints with 3, 2 and 2 degrees of freedom, respectively.

Walking velocity was calculated from kinematic data. The external knee joint moments were computed using inverse dynamics following a recursive Newton-Euler method[25] in Visual3D (V5, C-Motion Inc., USA) and expressed in the shank coordinate system. Moments, normalized to body mass (Nm/kg), were reported as the mean of the three successful trials per participant. Data were time-normalised to 101 points representing 0 to 100% of the stance phase. The knee moments included: peak knee flexion (KFM), terminal stance peak knee extension (KEM), peak knee adduction (KAM, first (KAM_1) and second (KAM_2) peaks), external (ERM) and internal rotation (IRM) moments (Fig. 1)[26]. The KAM impulse, representing the area under the adduction moment curve, was computed using the trapezoidal method across the entire stance phase. The tibiofemoral total joint reaction force

(JRF) was computed using a musculoskeletal model based on the geometry of Delp et al.[27] as described in detail previously[24] using MATLAB (R2013a, Mathworks, Inc., Natick, MA, USA) and normalized to body weights.

2.3 Clinical and radiographic data (disease severity and joint alignment)

The Western Ontario & McMaster Universities Osteoarthritis Index (WOMAC) (5 point Likert-type format) was completed by each participant during the biomechanics laboratory visit, to assess the degree of self-reported knee pain and functional limitation[28]. Mechanical alignment (mechanical axis deviation (MAD), medial proximal tibial angle (MPTA)) and OA disease severity (Kellgren-Lawrence Grading[29], OARSI Atlas[30]) of the affected joint, were evaluated from full-length anterior-posterior weight-bearing radiographs by an experienced examiner (LBS). MAD is defined as the perpendicular distance (in mm) from the knee joint centre to the mechanical axis, where the mechanical axis is the line connecting the centre of the femoral head to the centre of the ankle joint. *Valgus alignment* was defined as >0mm lateral deviation, *neutral alignment* between 0-15mm medial deviation and *varus alignment* as >15mm medial deviation[31]. The MPTA is defined as the medial angle between the anatomical axis of the tibia (line from knee centre to ankle centre) and a line parallel to the tibial plateau surface.

2.4 Micro-CT imaging and morphometric analysis

Tibial plateaus were retrieved following TKA and fixed in 70% ethanol solution. Specimens were scanned with a desktop micro-CT system (Skyscan 1076, Skyscan-Bruker, Kontich, Belgium) at 17.4µm isotropic pixel size, source voltage 100kVp, current 90µA, rotation step 0.4° over 180° rotation, exposure time 590ms, 4 frames averaging and 0.5 mm-thick aluminium filter for beam hardening reduction (further details in Roberts et al.[16,32]). Prior to scanning, specimens were removed from the ethanol solution and wrapped in cling-film. Scans were performed with the tibial plateau fixed on a carbon bed, with the medial-lateral axis of each specimen aligned with the system's rotation axis[16]. For each specimen, 4997 consecutive cross-section images were reconstructed (86.9mm length, slice thickness one pixel (17.4µm)) using a filtered back-projection algorithm, each image 3936x3936 pixels (68.5x68.5mm) in size and saved in 8-bit grayscale format (NRecon software, v1.6.9.8, Skyscan-Bruker, Kontich, Belgium). Cross-section images were then rotated in 3D and saved with the anatomical superior-inferior axis of each plateau aligned with the z-axis of the image stack (DataViewer software, v 1.5.1.2, Skyscan-Bruker, Kontich, Belgium)[16].

In each tibial plateau image dataset, four cylindrical STB volumes of interest (VOI) were selected within the load bearing regions of the tibial condyles; each VOI was centred within the anterior or posterior halves of the medial and lateral condyles, which were defined by elliptical regions (Fig. 2a): anteromedial (AM), posteromedial (PM), anterolateral (AL) posterolateral (PL) VOI[32]. The cylindrical VOIs contained only subchondral trabecular bone, were of diameter 10mm and minimum length 3mm (to satisfy the continuum assumption of trabecular bone[33,34]), maximum 5mm, depending on the specimen. The superior surface of each VOI was subjacent to the inferior surface of the subchondral bone plate, extending distally towards the growth plate (Fig. 2b). Each STB VOI was binarised with uniform thresholding[35,36] and the following morphometric parameters were calculated for each volume (software CT Analyser, v1.14.4.1)[16]: bone volume fraction (BV/TV, %), ratio of the voxels segmented as bone to the total number of voxels constituting the examined VOI[37]; trabecular thickness (Tb.Th, mm), average 3D thickness of the trabeculae within examined VOI[38,39]; trabecular separation (Tb.Sp, mm), 3D measure of the mean distance between the trabeculae within the VOI[38]; trabecular number (Tb.N, 1/mm), the number of trabeculae per unit length[37]; structure model index (SMI, *unitless*), parameter describing the ratio of rod- to plate-like trabecular structures within examined VOI (value range: from 0 (ideal plate-like structure) to 3 (ideal rod-like structure))[39,40].

The medial (M) and lateral (L) condyle BV/TV were computed as the average BV/TV of the anterior (A) and posterior (P) VOIs within each condyle. The BV/TV ratios within each condyle (anterior-to-posterior, A:P) and between the condyles (medial-to-lateral, M:L) were also computed.

2.5 Statistics

A power analysis (G*Power 3.1[41]) indicated that for a statistical power= 0.8 and alpha= 0.05, a minimum sample size of 17 patients would be necessary for detecting significant differences (effect size of 1 standard deviation) among STB subregions and significant associations (effect size r=0.6) between knee loading and STB microarchitectural parameters.

Differences in the five morphometric parameters (BV/TV, SMI, Tb.Th, Tb.N and Tb.Sp) among the four tibial subregions (AM, PM, AL, PL) were assessed by using five independent repeated measures ANOVA, followed by paired t-test with Bonferroni adjustment for multiple comparisons. Independent ANOVAs were conducted, instead of a single MANOVA, due to strong interrelationships among the morphometric parameters investigated ($r>0.8$). For each ANOVA, Bonferroni correction for 30 total comparisons (6 subregional comparisons per parameter) was applied at alpha= 0.05 (effective p-value=0.0017 for significance). STB parameters were tested for assumptions of normality and sphericity, with departures from sphericity corrected using the Greenhouse-Geisser method[42].

Linear relationships between STB subregional microarchitecture parameters, BV/TV ratios, dynamic joint loads and knee alignment parameters were examined using Pearson's correlations with subsequent Benjamini-Hochberg adjustment (false discovery rate=0.05), to control for multiple testing[43]. Then, to control for potentially confounding variables that influence the medial JRF or the medial-to-lateral load distribution, multiple linear regression analysis was performed, for predicting AM BV/TV or M:L BV/TV ratios, respectively. The ERM, which was the loading index most strongly correlated with the dependent variables (AM BV/TV and M:L BV/TV ratio), was forward entered into multiple regression models, considering walking speed, KAM_1, and MAD as covariates[19,20,44]. STB microarchitecture and joint loading parameters were tested for assumptions of normality (Shapiro-Wilks test), homogeneity of variance (Levene's test), linearity, multicollinearity (variance inflation factor) and homoscedasticity (scatter plot of residuals). The significance level was set to $p<0.05$. Statistical analysis was performed using SPSS Statistics 22 (IBM Corp., Armonk, NY, USA).

A secondary analysis (Supplementary Materials) was performed, subdividing the cohort in two subgroups: one with neutrally to varus-aligned joints (constituting the “neutral-varus” group, MAD >0 mm) and one with valgus-aligned joints (MAD <0 mm)[31]. The neutral-varus subgroup enables comparison with previous literature, as relationships between joint loading and proximal tibial BMD were exclusively explored in medial knee OA patients[11,13], whereas relationships for valgus subgroup, to the best of our knowledge, are reported for the first time.

3. Results

Patient characteristics, radiographic features and gait data are reported in Table 1, Table 2 and Fig. 1, respectively. Of the 25 patients examined, 15 exhibited varus, three neutral and seven valgus joint alignment (Table 1). For the secondary analysis (Supplementary Materials for more details), the neutral and the varus patients whom all presented with medial knee OA were then merged, constituting the “neutral-varus” subgroup (n=18). Two VOIs (one PM and one PL VOI from separate patients) were excluded from analysis, as these VOIs were too thin (VOI height <3 mm).

3.1 Tibial subchondral trabecular bone microarchitecture

In the entire OA cohort, significant differences (ANOVA, $p<0.001$) in bone morphometric parameters were found among the four anatomical VOIs (Fig. 3). The AM VOI had the highest BV/TV and Tb.N (up to +75% [45%,104%] (mean difference [95% confidence interval] and +41% [22%,59%], respectively) and lowest SMI (up to -69% [-36%,-68%]) compared with the other regions, with largest differences to the AL VOI (Fig. 2c,d). AM Tb.Th was higher (up to +26% [16%,36%]) and AM Tb.Sp lower (up to -25% [-15%,-35%]) compared with the AL and PL VOIs. STB microarchitecture did not significantly differ between the AL and PL VOIs, in any parameter.

3.2 Relationships between knee joint loading and tibial subchondral trabecular bone microarchitecture

Indices of joint loading were significantly correlated with regional tibial 3D microarchitectural parameters (Fig. 4). Among these, ERM was most strongly correlated with medial STB microarchitecture, negatively with AM BV/TV (r=-0.74 [-0.48,-0.88], Fig. 5a), M BV/TV (r=-0.69 [-0.40,-0.85]) and positively with the AM SMI (r=0.67 [0.38,0.84]). MAD correlated significantly with lateral STB microarchitecture, most strongly with BV/TV (PL, r=-0.71 [-0.40,-0.87], Fig. 5b; L, r=-0.71 [-0.41,-0.87]; AL, r=-0.68 [-0.36,-0.85]). Remaining loading indices were weaker and not significantly associated with any microarchitectural parameter, except for KEM which correlated with AL Tb.Sp and Tb.N (r=0.72 [0.45,0.87], and r=-0.57 [-0.22,-0.78], respectively).

3.3. Relationships between knee joint loading and tibial BV/TV ratios among subregions

Indices of knee joint loading significantly correlated with BV/TV ratios among subregions (Fig. 4). Medial-to-lateral BV/TV ratios (M:L, AM:PL, PM:AL and PM:PL ratios) were most strongly associated, negatively with ERM and positively with MAD. The strongest correlations were "M:L BV/TV vs. ERM" (r=-0.74 [-0.48,-0.88], Fig. 5c) and "M:L BV/TV vs. MAD" (r=0.74 [0.45,0.88], Fig. 5d); for all other ratios, |r|-range: 0.57–0.71, p<0.05 for all). The M:L BV/TV ratio was also significantly associated with, in order of descending strength, the KAM_1, KAM, KAM_2, IRM and KAM impulse (|r|-range: 0.54–0.60). No significant associations were observed between measures of joint loading and anterior-to-posterior (AM:PM, AL:PL) BV/TV ratios.

3.4 Stepwise Multiple Linear Regression Analysis

ERM entered all regression models for prediction of AM BV/TV or M:L BV/TV ratio, after controlling for walking speed, KAM_1 and MAD (Table 3). The ERM explained additional 26-30% of the variation in AM BV/TV (final model: walking speed, MAD, KAM, ERM, adjusted $R^2=0.59$, $p=0.001$) and additional 11% in M:L BV/TV ratio (final model: MAD, KAM, ERM, adjusted $R^2=0.69$, $p<0.0005$), compared to these regression model without ERM (adjusted $R^2=0.27$ and adjusted $R^2=0.53$, respectively). One patient, assessed against the standardized residuals, leverage and Cook's Distance, was considered influential and thus was removed from each regression model. Multicollinearity was considered a minor problem, despite strong association between KAM_1 and MAD (r=-0.83, Supplementary Material), as variance inflation factor was < 4.4 for all models[45].

4. Discussion

This exploratory study performed, on the same patient, a combination of 3D gait analysis and micro-CT imaging to investigate relationships between knee joint loading indices and subregional measurements of proximal tibial STB microarchitecture in end-stage knee OA. STB microarchitecture differed significantly among condylar subregions, with highest BV/TV and more plate-like structure anteromedially. The STB microarchitecture in the medial condyle, particularly in the AM compartment, was most strongly associated with ERM during early stance, whereas laterally it was most strongly associated with MAD. The M:L BV/TV subregional ratios were also significantly and most strongly associated with ERM and MAD, followed by KAM indices and IRM. ERM explained additional variation in AM BV/TV and M:L BV/TV ratio when controlling for KAM_1 and MAD in multiple linear regression models. However, one might consider the possibility that the associations with ERM could be an artefact of the cross-sectional study design, since ERM was an order of magnitude lower than other moments examined, and that the majority of ERM measures were below the threshold of accuracy.

Frontal plane loading indices were associated with the M:L BV/TV ratio, most strongly with static alignment (MAD), followed by associations with KAM_1, KAM_2 and KAM impulse; these findings are consistent with previous reports on associations between knee loads and DXA-measures of proximal tibia BMD ratios (analogous with the BV/TV ratios here)[11,13]. The MAD was also the parameter most strongly correlated with lateral STB microarchitecture, particularly with AL and PL BV/TV, Tb.Th and Tb.N. The stronger associations "MAD vs. M:L BV/TV" compared with "KAM vs. M:L BV/TV" are consistent with previous findings using BMD[13]. However, M:L BV/TV ratio correlated stronger with peak KAM indices (discrete measures of loading) than with the KAM impulse (a cumulative measure of load during stance), which is different to what has been found previously[13]. Overall, all the associations reported herein between joint loading indices and measures of bone quantity were stronger (|r|-range: 0.54-0.74) compared with previously published work in patients with medial knee OA (|r|-range: 0.30-0.53)[11,13]. Importantly, the present study differs from previous work by employing micro-CT rather than DXA, permitting examination of the STB microarchitecture in specific subregions of the proximal tibia, where microarchitectural differences with OA are most evident and hence could, in part, explain the stronger associations[14].

Peak rotational moments were strongly associated with subregional STB microarchitecture for "ERM vs. AM (and M) BV/TV" and "ERM vs. AM SMI", with a positive and negative sign, respectively; anteromedially being the anatomical location where BV/TV was highest and SMI lowest in the present OA series. Furthermore, ERM was the dynamic loading parameter most strongly associated with M:L BV/TV ratio overall (same strength as the static loading index MAD); the internal rotational moment correlated also significantly ("IRM vs. M:L BV/TV"), however, weaker. Interestingly, in a multiple regression model, the ERM explained additional variation in the AM BV/TV and M:L BV/TV ratio, when controlling for walking speed, KAM_1 and MAD, parameters that influence tibial JRF[19]. In OA patients, gait studies have documented lower[3,46], or non-statistically different ERM, compared to controls[47]; further, no significant changes in ERM were observed in OA following surgical intervention (high tibial osteotomy)[48,49]. However, its association with variations in knee bone structure, had not yet been explored. Hence, the significance of rotational moments to overall loading at the knee joint remains currently uncertain. We acknowledge the relatively poor measurement reliability in these transverse plane loading indices; it is unclear, given their low magnitude, whether the rotational moments observed (Fig. 5a,c) are within measurement accuracy thresholds. This limitation possibly accounting for discrepancies among studies[46,48,50]. Further, results on rotational moments should be considered within this context. If confirmed, these findings could suggest that the rotational moments during early stance may be useful parameters for describing variations in the STB bone across the tibial plateau, beyond frontal loading indices. Further, it supports previous evidence that this early period of stance, characterized by changes in joint function in OA (e.g. increased muscle co-activity[51], joint stiffness[52]), is important in disease pathomechanics.

Finally, the JRF was not significantly associated neither with subregional STB microarchitecture, nor with BV/TV subregional ratios. One reason for this absence of significant associations may be due to the used musculoskeletal model computing the overall JRF, rather than medial or lateral condyle-specific JRF, hence not giving a measure of the M:L load distribution. Furthermore, the model assumes non-pathological muscle activation patterns, thus not accounting for differences in loading that may be due to variations in muscle activity in knee OA[53].

The scientific literature suggests that beside bone density (BV/TV), subchondral bone microarchitecture (including SMI) varies in human knee OA, depending on stage of the disease[14,54] and joint alignment[16]. In early OA (mouse models), subchondral bone erosion (decreased BV/TV values and more rod-like structures compared to baseline) has been reported, whereas in late OA (in mice and in human OA), trabecular bone thickening with sclerosis (very high BV/TV values) and more plate-like structures, particularly in the medial condyle, has been observed[14,55]. However, no human gait analysis was performed in these studies. Hence, to the best of the authors' knowledge, this study is the first to explore associations between peak moments and variations in joint bone microarchitecture in the same patient.

The results presented should be interpreted within the limitations of this study. A major limitation was the small sample size, given the many associations examined. Benjamini-Hochberg correction was applied, to account for multiple testing. Given we allow for a false discovery rate of 5% (Type I error), future studies are required to confirm the observed relationships in bigger cohorts. Second, due to the cross-sectional study design, it is also unclear whether the joint loads observed in these patients just prior to TKA reflect knee loads that also occur during earlier stages of the disease and that may have influenced the resultant bone microarchitecture observed within this study. Certainly, walking speed in our end-stage OA patients, which is known to affect the magnitude of peak knee moments[19], was slower (almost halved, 0.70 ms^{-1}) than reported in patients with less severe OA (1.1-1.3 ms^{-1})[3,13,47]. Moreover, we cannot exclude in the present sample, that other factors, apart from loading, including age, genetics, or the local biochemical environment in the presence of bone sclerosis (Table 2), affect subchondral bone metabolism[55]. Hence, we could not determine whether the revealed relationships between joint loading and STB microarchitecture are present in the earlier stages of the disease, or within non-pathological joints. Micro-CT cannot currently be applied *in vivo* on human knees for characterisation of STB microarchitecture, thus this study was restricted to patients who underwent TKA due to knee OA. However, recent high-resolution peripheral quantitative CT (HR-pQCT) imaging systems, permitting *in vivo* examination of proximal tibial STB microarchitecture with 61µm voxel size[56], may in future be employed to examine the above relationships, using the image analysis methods described herein, in early OA and non-pathological joints. HR-pQCT may also be useful for examining whether longitudinal changes in STB microarchitecture can be explained by baseline measures of joint loading. Moreover, we did not study articular cartilage morphology, for example cartilage thickness, which is important in load transfer across the tibiofemoral joint. Lastly, variations in radiographic disease severity (mild to severe) and knee joint alignment (varus to valgus) could also be drivers of associations between joint loading indices and bone microarchitecture observed herein; the former suggested by previously published literature[13], the latter (varus to valgus) suggested by our subgroup analysis (Supplementary Materials), for which we acknowledge the small sample size. As medial and lateral OA may represent distinct disease phenotypes[57], the investigation of each subgroup of appropriate sample size in future is warranted.

The strength of this study is the combination of 3D micro-CT and gait analysis, on the same patient. This permits examination of the STB microarchitecture in specific subregions of the proximal tibial plateau, where microarchitectural differences with OA are most evident, combining them with *in vivo* measures of joint loading of the same subject. Moreover, as the micro-CT examination was performed on entire tibial plateaus without coring, specimens are preserved intact for further examination[16].

Concluding, although not definitive in light of the small sample size, this study in end-stage knee OA patients suggests that dynamic and static indices of knee joint loading are significantly associated with regional variations in 3D subchondral trabecular bone microarchitecture. These novel findings may contribute to a better understanding of the distribution of joint loads upon the tibial plateau and its possible links with bone microarchitecture in late stage OA. Future work may confirm these in a bigger cohort and elucidate, if present, causative links between joint loading and STB microarchitectural changes, to identify potential biomechanical factors that may be targets for surgical or non-invasive therapies.

Acknowledgements

The authors thank statistician Pawel Skuza, Flinders University, for statistical assistance and Adelaide Microscopy for providing access to the micro-CT system. We also wish to thank Drs John Arnold and Francois Fraysse, University of South Australia, who assisted in recruitment of patients and collection of gait analysis data, and Annika Theodoulou, Repatriation General Hospital, and the staff at the Royal Adelaide Hospital for their assistance in the recruitment of patients for this study.

Author contributions

BCR contributed to data acquisition, study design, data analysis and interpretation, graphical representation, manuscript drafting. LBS, DT and EP contributed to the study design, data acquisition and interpretation, manuscript drafting, critical revision of this manuscript and sourced funding for this project. GM and KJR were involved in study design, interpretation of data and critical revision of this manuscript and sourced funding for this project. All authors approved the final version of the manuscript to be published. BCR, DT and EP take full responsibility for the integrity of this work as a whole, from inception to finished article (bryant.roberts@flinders.edu.au, dominic.thewlis@adelaide.edu.au, egon.perilli@flinders.edu.au).

Role of the funding source

Funding for this study was provided by Grant in Aid (2013), Arthritis Australia-Zimmer Australia and Catalyst Grant DSD (2013), Premier's Research and Industry Fund, Government of South Australia. Dominic Thewlis receives fellowship funding from the NHMRC (ID: 1126229). The funding bodies had no role in the study design; collection, analysis and interpretation of data; writing of this report and decision to submit this article for publication.

Conflict of interest

None

References

1. Madry H, van Dijk CN, Mueller-Gerbl M. The basic science of the subchondral bone. Knee Surg Sports Traumatol Arthrosc 2010;18(4):419-33.
2. Radin EL, Rose RM. Role of subchondral bone in the initiation and progression of cartilage damage. Clin Orthop Relat Res 1986;213:34-40.
3. Landry SC, McKean KA, Hubley-Kozey CL, Stanish WD, Deluzio KJ. Knee biomechanics of moderate OA patients measured during gait at a self-selected and fast walking speed. J Biomech 2007;40(8):1754-61.
4. Astephen JL, Deluzio KJ, Caldwell GE, Dunbar MJ. Biomechanical changes at the hip, knee, and ankle joints during gait are associated with knee osteoarthritis severity. J Orthop Res 2008;26(3):332-41.
5. Sharma L, Song J, Felson DT, Cahue S, Shamiyeh E, Dunlop DD. The role of knee alignment in disease progression and functional decline in knee osteoarthritis. JAMA 2001;286(2):188-95.
6. Miyazaki T, Wada M, Kawahara H, Sato M, Baba H, Shimada S. Dynamic load at baseline can predict radiographic disease progression in medial compartment knee osteoarthritis. Ann Rheum Dis 2002;61(7):617-22.

7. Creaby MW, Wang Y, Bennell KL, Hinman RS, Metcalf BR, Bowles KA, et al. Dynamic knee loading is related to cartilage defects and tibial plateau bone area in medial knee osteoarthritis. Osteoarthritis Cartilage 2010;18(11):1380-5.
8. Bennell KL, Creaby MW, Wrigley TV, Bowles K-A, Hinman RS, Cicuttini F, et al. Bone marrow lesions are related to dynamic knee loading in medial knee osteoarthritis. Ann Rheum Dis 2010;69(6):1151-4.
9. Vanwanseele B, Eckstein F, Smith R, Lange A, Foroughi N, Baker M, et al. The relationship between knee adduction moment and cartilage and meniscus morphology in women with osteoarthritis. Osteoarthritis Cartilage 2010;18(7):894-901.
10. Andriacchi TP, Koo S, Scanlan SF. Gait mechanics influence healthy cartilage morphology and osteoarthritis of the knee. J Bone Joint Surg Am 2009;91:95-101.
11. Wada M, Maezawa Y, Baba H, Shimada S, Sasaki S, Nose Y. Relationships among bone mineral densities, static alignment and dynamic load in patients with medial compartment knee osteoarthritis. Rheumatology (Oxford) 2001;40(5):499-505.
12. Hurwitz DE, Sumner DR, Andriacchi TP, Sugar DA. Dynamic knee loads during gait predict proximal tibial bone distribution. J Biomech 1998;31(5):423-30.
13. Thorp LE, Wimmer MA, Block JA, Moisio KC, Shott S, Goker B, et al. Bone mineral density in the proximal tibia varies as a function of static alignment and knee adduction angular momentum in individuals with medial knee osteoarthritis. Bone 2006;39(5):1116-22.
14. Patel V, Issever AS, Burghardt A, Laib A, Ries M, Majumdar S. MicroCT evaluation of normal and osteoarthritic bone structure in human knee specimens. J Orthop Res 2003;21(1):6-13.
15. Bobinac D, Spanjol J, Zoricic S, Maric I. Changes in articular cartilage and subchondral bone histomorphometry in osteoarthritic knee joints in humans. Bone 2003;32(3):284-90.
16. Roberts BC, Thewlis D, Solomon LB, Mercer G, Reynolds KJ, Perilli E. Systematic mapping of the subchondral bone 3D microarchitecture in the human tibial plateau: Variations with joint alignment. J Orthop Res 2016;35(9):1927-41.
17. Perilli E, Briggs AM, Kantor S, Codrington J, Wark JD, Parkinson IH, et al. Failure strength of human vertebrae: prediction using bone mineral density measured by DXA and bone volume by micro-CT. Bone 2012;50(6):1416-25.
18. Ab-Lazid R, Perilli E, Ryan MK, Costi JJ, Reynolds KJ. Does cancellous screw insertion torque depend on bone mineral density and/or microarchitecture? J Biomech 2014;47(2):347-53.
19. Kutzner I, Trepczynski A, Heller MO, Bergmann G. Knee adduction moment and medial contact force--facts about their correlation during gait. PLoS One 2013;8(12):e81036.
20. Schipplein O, Andriacchi T. Interaction between active and passive knee stabilizers during level walking. J Orthop Res 1991;9(1):113-9.
21. Cappozzo A, Catani F, Della Croce U, Leardini A. Position and orientation in space of bones during movement: anatomical frame definition and determination. Clin Biomech (Bristol, Avon) 1995;10(4):171-8.
22. Winter DA. Biomechanics and motor control of human movement. 4th Edition. Hoboken, NJ, USA, John Wiley & Sons 2009.
23. Lu T-W, O'connor J. Bone position estimation from skin marker co-ordinates using global optimisation with joint constraints. J Biomech 1999;32(2):129-34.
24. Thewlis D, Callary SA, Fraysse F, Solomon LB. Peak loading during walking is not associated with fracture migration following tibial plateau fracture: A preliminary case series. J Orthop Res 2015;33(9):1398-406.
25. Doriot N, Chèze L. A three-dimensional kinematic and dynamic study of the lower limb during the stance phase of gait using an homogeneous matrix approach. IEEE Trans Biomed Eng 2004;51(1):21-7.
26. Zabala ME, Favre J, Scanlan SF, Donahue J, Andriacchi TP. Three-dimensional knee moments of ACL reconstructed and control subjects during gait, stair ascent, and stair descent. J Biomech 2013;46(3):515-20.

27. Delp SL, Loan JP, Hoy MG, Zajac FE, Topp EL, Rosen JM. An interactive graphics-based model of the lower extremity to study orthopaedic surgical procedures. IEEE Trans Biomed Eng 1990;37(8):757-67.
28. Bellamy N, Buchanan WW, Goldsmith CH, Campbell J, Stitt LW. Validation study of WOMAC: a health status instrument for measuring clinically important patient relevant outcomes to antirheumatic drug therapy in patients with osteoarthritis of the hip or knee. J Rheumatol 1988;15(12):1833-40.
29. Kellgren J, Lawrence J. Radiological assessment of osteo-arthrosis. Ann Rheum Dis 1957;16(4):494-502.
30. Altman RD, Gold GE. Atlas of individual radiographic features in osteoarthritis, revised. Osteoarthr Cartilage 2007;15:A1-A56.
31. Paley D. Principles of deformity correction. Berlin, Heidelberg, Springer 2002.
32. Roberts BC, Solomon LB, Mercer G, Reynolds KJ, Thewlis D, Perilli E. Joint loading and proximal tibia subchondral trabecular bone microarchitecture differ with walking gait patterns in end-stage knee osteoarthritis. Osteoarthr Cartilage 2017;25(10):1623-32.
33. Harrigan TP, Jasty M, Mann RW, Harris WH. Limitations of the continuum assumption in cancellous bone. J Biomech 1988;21(4):269-75.
34. Tassani S, Perilli E. On local micro-architecture analysis of trabecular bone in three dimensions. Int Orthop 2013;37(8):1645-6.
35. Perilli E, Baruffaldi F, Visentin M, Bordini B, Traina F, Cappello A, et al. MicroCT examination of human bone specimens: effects of polymethylmethacrylate embedding on structural parameters. J Microsc 2007;225(2):192-200.
36. Perilli E, Baleani M, Öhman C, Baruffaldi F, Viceconti M. Structural parameters and mechanical strength of cancellous bone in the femoral head in osteoarthritis do not depend on age. Bone 2007;41(5):760-8.
37. Perilli E, Parkinson IH, Reynolds KJ. Micro-CT examination of human bone: from biopsies towards the entire organ. Ann Ist Super Sanita 2012;48(1):75-82.
38. Hildebrand T, Rüegsegger P. A new method for the model-independent assessment of thickness in three-dimensional images. J Microsc 1997;185(1):67-75.
39. Perilli E, Baruffaldi F, Bisi M, Cristofolini L, Cappello A. A physical phantom for the calibration of three-dimensional X-ray microtomography examination. J Microsc 2006;222(2):124-34.
40. Hildebrand T, Rüegsegger P. Quantification of bone microarchitecture with the structure model index. Comput Methods Biomech Biomed Engin 1997;1(1):15-23.
41. Faul F, Erdfelder E, Buchner A, Lang A-G. Statistical power analyses using G* Power 3.1: Tests for correlation and regression analyses. Behav Res Methods 2009;41(4):1149-60.
42. Greenhouse SW, Geisser S. On methods in the analysis of profile data. Psychometrika 1959;24(2):95-112.
43. Benjamini Y, Hochberg Y. Controlling the false discovery rate: a practical and powerful approach to multiple testing. Journal of the royal statistical society Series B (Methodological) 1995:289-300.
44. Adouni M, Shirazi-Adl A. Partitioning of knee joint internal forces in gait is dictated by the knee adduction angle and not by the knee adduction moment. J Biomech 2014;47(7):1696-703.
45. Hair JF, Black WC, Babin BJ, Anderson RE, Tatham RL. Multivariate data analysis. Volume 5, Prentice hall Upper Saddle River, NJ 1998.
46. Richardson SE. Reliability and validity of knee moments: 3D gait analysis in subjects with and without knee osteoarthritis. vol. MSc: Western University 2012.
47. Kaufman KR, Hughes C, Morrey BF, Morrey M, An K-N. Gait characteristics of patients with knee osteoarthritis. J Biomech 2001;34(7):907-15.
48. Leitch KM, Birmingham TB, Dunning CE, Giffin JR. Medial opening wedge high tibial osteotomy alters knee moments in multiple planes during walking and stair ascent. Gait Posture 2015;42(2):165-71.

49. Leitch KM, Birmingham TB, Dunning CE, Giffin JR. Changes in valgus and varus alignment neutralize aberrant frontal plane knee moments in patients with unicompartmental knee osteoarthritis. J Biomech 2013;46(7):1408-12.
50. Robbins SM, Wilson JLA, Rutherford DJ, Hubley-Kozey CL. Reliability of principal components and discrete parameters of knee angle and moment gait waveforms in individuals with moderate knee osteoarthritis. Gait Posture 2013;38(3):421-7.
51. Childs JD, Sparto PJ, Fitzgerald GK, Bizzini M, Irrgang JJ. Alterations in lower extremity movement and muscle activation patterns in individuals with knee osteoarthritis. Clin Biomech (Bristol, Avon) 2004;19(1):44-9.
52. Zeni JA, Higginson JS. Dynamic knee joint stiffness in subjects with a progressive increase in severity of knee osteoarthritis. Clinical biomechanics 2009;24(4):366-71.
53. Heiden TL, Lloyd DG, Ackland TR. Knee joint kinematics, kinetics and muscle co-contraction in knee osteoarthritis patient gait. Clin Biomech (Bristol, Avon) 2009;24(10):833-41.
54. Ding M, Odgaard A, Hvid I. Changes in the three-dimensional microstructure of human tibial cancellous bone in early osteoarthritis. J Bone Joint Surg Br 2003;85(6):906-12.
55. Li G, Yin J, Gao J, Cheng TS, Pavlos NJ, Zhang C, et al. Subchondral bone in osteoarthritis: insight into risk factors and microstructural changes. Arthritis Res Ther 2013;15(6):223.
56. Kroker A, Zhu Y, Manske SL, Barber R, Mohtadi N, Boyd SK. Quantitative in vivo assessment of bone microarchitecture in the human knee using HR-pQCT. Bone 2016.
57. Waarsing JH, Bierma-Zeinstra SM, Weinans H. Distinct subtypes of knee osteoarthritis: data from the Osteoarthritis Initiative. Rheumatology (Oxford) 2015:kev100.

Figure 1 Average external knee moments and standard deviation (shaded area) over the stance phase of the gait cycle for all knee OA patients ($n = 25$). Reported peak knee moments are highlighted: KFM: knee flexion moment, KEM: knee extension moment, KAM_1, KAM_2: first and second peak knee adduction moments, ERM: external rotation moment, IRM: internal rotation moment.

Figure 2 (a) 3D micro-CT image of an excised tibial plateau from a right knee (view from top). The ellipses defining the medial and lateral tibial condyles are shown (dashed lines), containing the location of the four subvolumes of interest (VOIs, as indicated by red circles) in the anterior-medial (AM), anterior-lateral (AL), posterior-medial (PM) and posterior-lateral (PL) compartments; **(b)** 2D coronal micro-CT cross-section image of the tibial plateau with medial and lateral boundaries of the ellipses indicated by red lines. The location of the subchondral trabecular AM and AL VOIs are indicated; **(c,d)** 3D micro-CT images of the cylindrical subchondral trabecular bone VOIs examined (10 mm diameter, 3 mm length), **(c)** specimen from the AM subregion showing high BV/TV and plate-like microarchitecture (BV/TV= 42%, SMI= 0.4); **(d)** specimen from the AL subregion showing low BV/TV and mainly rod-like microarchitecture (BV/TV= 13%, SMI= 2.2).

Figure 3 Univariate scatter plots reporting values of 3D subchondral trabecular bone morphometric parameters in the four subregions of interest within the proximal tibial plateau, for all OA patients ($n = 25$). Mean and standard deviation (error bars) indicated. AM: anterior-medial, AL: anterior-lateral, PM: posterior-medial, PL: posterior-lateral, BV/TV: bone volume fraction, SMI: structure model index, Tb.Th: trabecular thickness, Tb.N, trabecular number, Tb.Sp: trabecular separation. Significant differences among the regions are indicated by lines ($p < 0.05$, paired t-test with Bonferroni adjustment).

Figure 4 Entire OA cohort (n = 25): Heatmap of Pearson's correlation coefficients (r-values) for "knee joint loads vs. subregional subchondral trabecular bone microarchitecture parameters and subregional BV/TV ratios". *Significant correlations (Benjamini-Hochberg adjusted, false discovery rate = 0.05) indicated. BV/TV: bone volume fraction, SMI: structure model index, Tb.Th: trabecular thickness, Tb.Sp: trabecular separation, Tb.N: trabecular number, AM: anterior-medial, AL: anterior-lateral, PM: posterior-medial, PL: posterior-lateral, KFM: knee flexion moment, KEM: knee extension moment, KAM: knee adduction moment, ERM: external rotation moment, IRM: internal rotation moment, JRF: joint reaction force, MAD: mechanical axis deviation, MPTA: medial proximal tibia angle.

Figure 5 Scatter plot with best fit line (solid line) and 95% confidence interval (dashed line) for Pearson's correlations: (a) "AM BV/TV vs. ERM", (b) "PL BV/TV vs. MAD", (c) "M:L BV/TV ratio vs. ERM" and (d) "M:L BV/TV ratio vs. MAD", for all OA patients (n = 25).

Table 1 Summary of physical characteristics and gait parameters of total knee arthroplasty patients (n = 25)

Age (years)	68 ± 7
Gender (male:females)	11:14
Affected limb (right:left)	13:12
Height (m)	1.66 ± 0.09
Body mass (kg)	91.6 ± 18.0
BMI (kg/m^2)	32.9 ± 4.4
WOMAC (total)	56 ± 13
Pain	12 ± 2
Stiffness	6 ± 1
Function	39 ± 12
Walking Speed (m/s)	0.70 ± 0.25
Knee moments (Nm/kg)	
Knee Flexion Moment, KFM	0.35 ± 0.23
Knee Extension Moment, KEM	-0.11 ± 0.29
First peak adduction moment, KAM_1	-0.40 ± 0.23
Second peak adduction moment, KAM_2	-0.39 ± 0.22
Knee adduction moment impulse	27.0 ± 14.2
External Rotation Moment, ERM	0.022 ± 0.023
Internal Rotation Moment, IRM	-0.085 ± 0.079
Joint reaction force (BW)	3.02 ± 0.96
Static Alignment	
Mechanical Axis Deviation (mm)	9.2 ± 34.8
Medial Proximal Tibial Angle (°)	90.1 ± 2.7

Average ± standard deviation. BW, bodyweights

Table 3 Summary of multiple linear regression analysis, for prediction of AM BV/TV and M:L BV/TV ratio

Dependent Var.	Model	Unadj. R^2	Adj. R^2	ΔR^2	p-value
AM BV/TV	MAD, KAM_1	0.285	0.206		0.049
	MAD, KAM_1, ERM	0.546	0.466	0.261*	0.003
	WS, MAD, KAM_1	0.371	0.266		0.036
	WS, MAD, KAM_1, ERM	0.668	0.590	0.297*	0.001
M:L BV/TV Ratio	MAD, KAM_1	0.588	0.529		0.001
	MAD, KAM_1, ERM	0.738	0.692	0.108*	< 0.0005

The external rotation moment (ERM), which was most strongly associated with the dependent variables, was forward entered into the regression models. Variables that influence the medial-to-lateral distribution (MAD, KAM_1) and/or medial condyle forces (WS, MAD, KAM_1) were input as covariates. *significant F-change, indicating ERM significantly improves prediction
BV/TV: bone volume fraction, AM: anterior-medial, M:L: medial-to-lateral ratio, WS: walking speed; MAD: mechanical axis deviation, KAM_1: first peak knee adduction moment

Table 2 Summary of knee radiographic features of all end-stage OA patients (n = 25)

Kellgren-Lawrence Grade	Grade	Number of subjects
	2	4
	3	7
	4	14

OARSI atlas radiographic features	Score	Number of subjects	
		Medial condyle	Lateral Condyle
Osteophyte	0	2	3
	1	13	14
	2	6	8
	3	4	0
Joint space narrowing	0	3	14
	1	5	6
	2	6	3
	3	11	2
Bone sclerosis	Present	13	6
	Absent	12	19

OA: osteoarthritis; OARSI: Osteoarthritis Research Society International.
All 13 patients exhibiting medial condyle bone sclerosis had varus-aligned joints (MAD >15 mm), whereas for the 6 patients with lateral sclerosis, 5 were valgus-aligned (MAD <0 mm) and one neutrally-aligned (MAD 0 - 15 mm).[30]

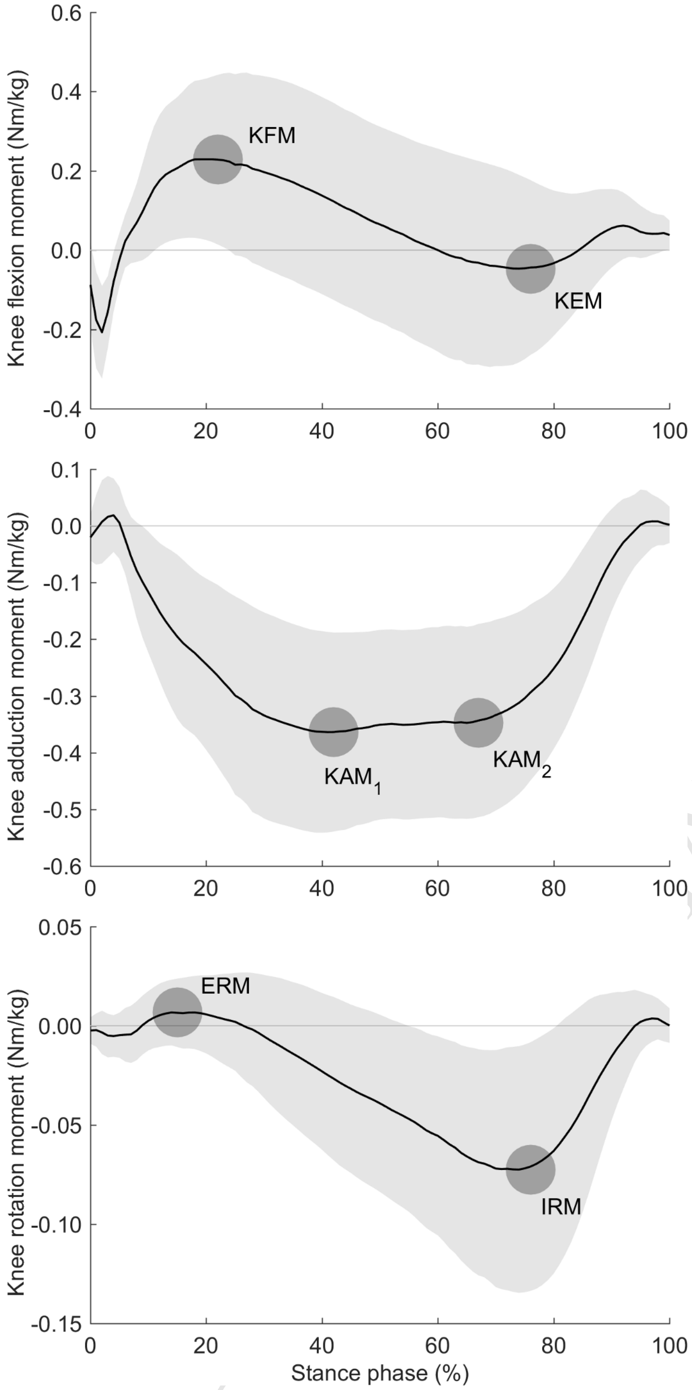

0.6
0.4
0.2
0.0
-0.2
-0.4
Knee flexion moment (Nm/kg)
KFM
KEM
0
20
40
60
80
100
0.1
0.0
-0.1
-0.2
-0.3
-0.4
-0.5
-0.6
Knee adduction moment (Nm/kg)
KAM1
KAM2
0.05
0.00
-0.05
-0.10
-0.15
Knee rotation moment (Nm/kg)
ERM
IRM
Stance phase (%)

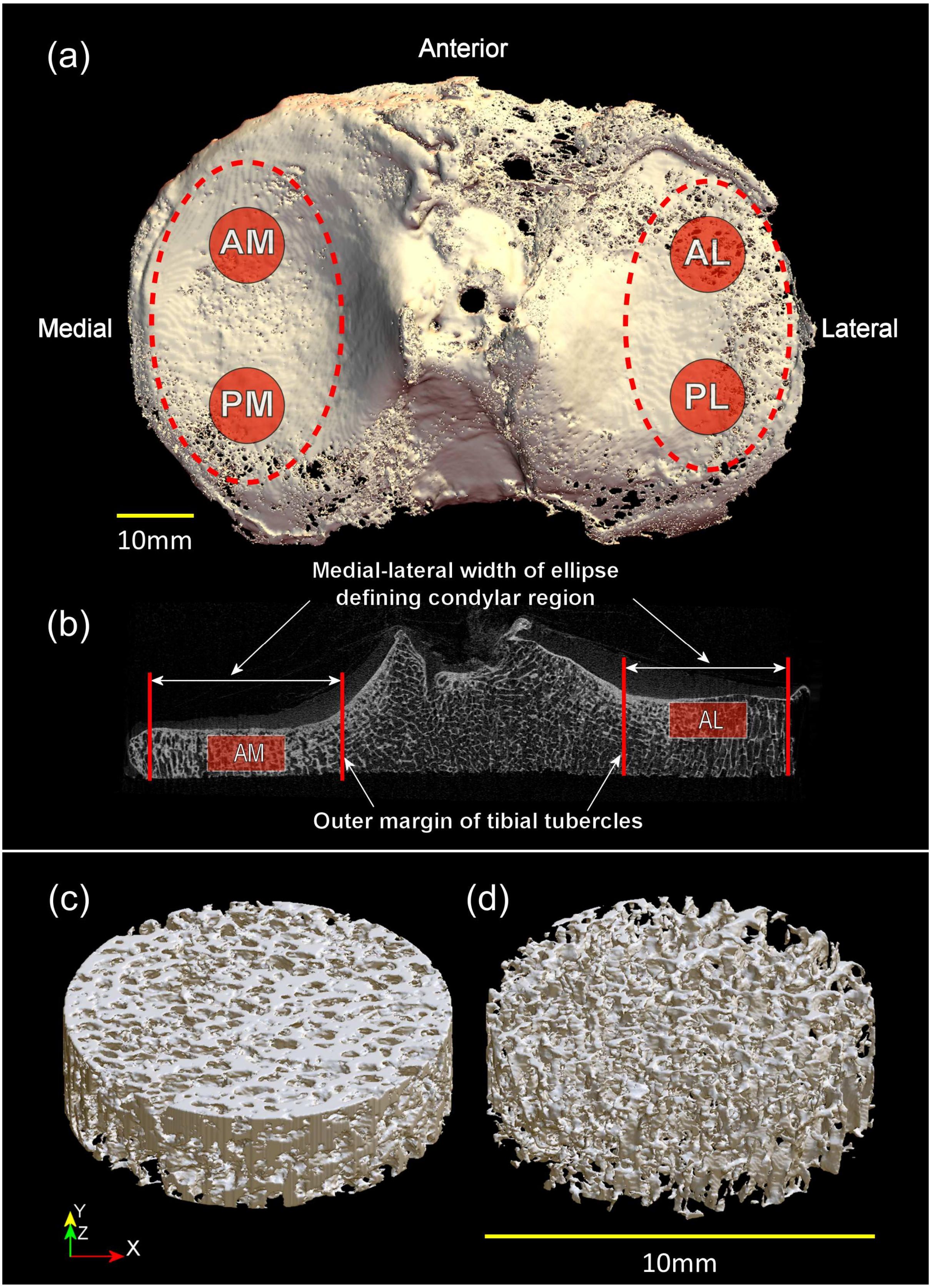
(a)
Anterior
AM
AL
Medial
Lateral
PM
PL
10mm
Medial-lateral width of ellipse
defining condylar region
(b)
AM
AL
Outer margin of tibial tubercles
(c)
(d)
Y
Z
X
10mm

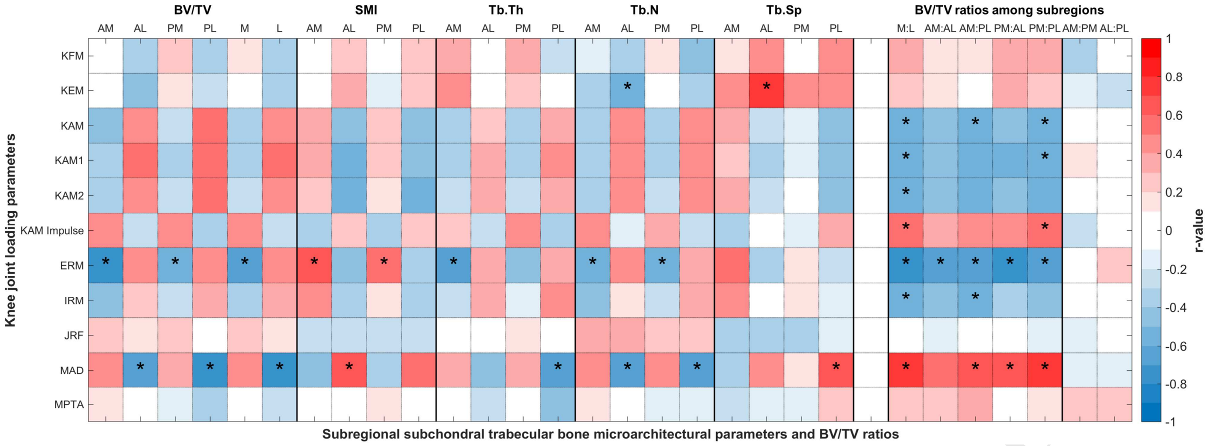
BV/TV
SMI
Tb.Th
Tb.N
Tb.Sp
BV/TV ratios among subregions
AM AL PM PL M L AM AL PM PL AM AL PM PL AM AL PM PL AM AL PM PL M:L AM:AL AM:PL PM:AL PM:PL AM:PM AL:PL
KFM
KEM
KAM
KAM1
KAM2
KAM Impulse
ERM
IRM
JRF
MAD
MPTA
Knee joint loading parameters
Subregional subchondral trabecular bone microarchitectural parameters and BV/TV ratios
r-value
1
0.8
0.6
0.4
0.2
0
-0.2
-0.4
-0.6
-0.8
-1

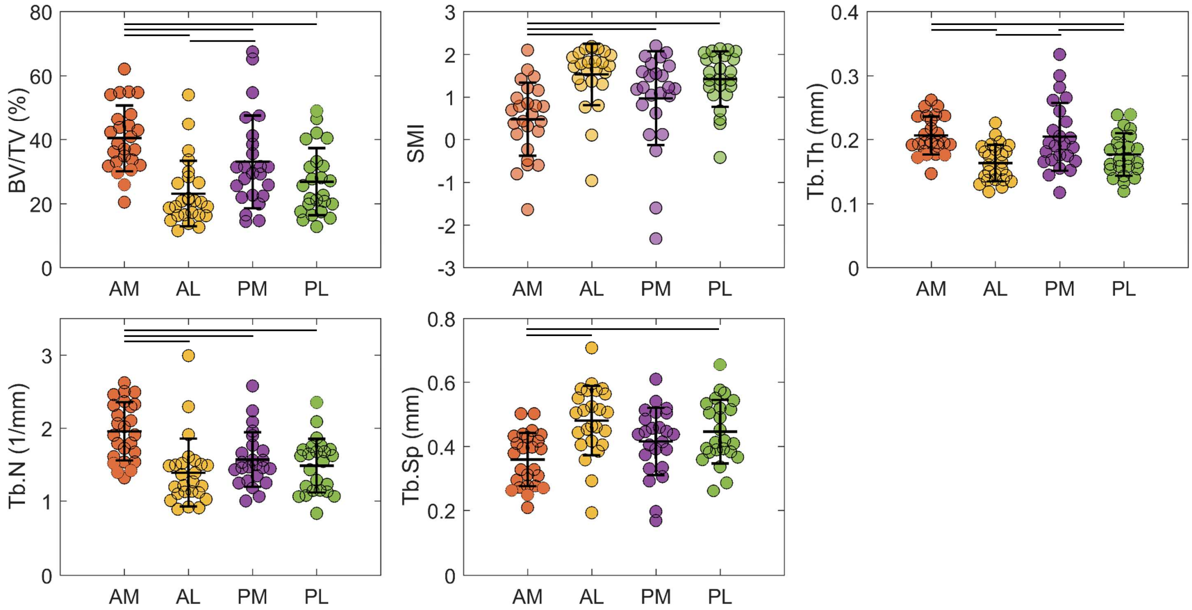

BV/TV (%)
SMI
Tb.Th (mm)
Tb.N (1/mm)
Tb.Sp (mm)
AM
AL
PM
PL

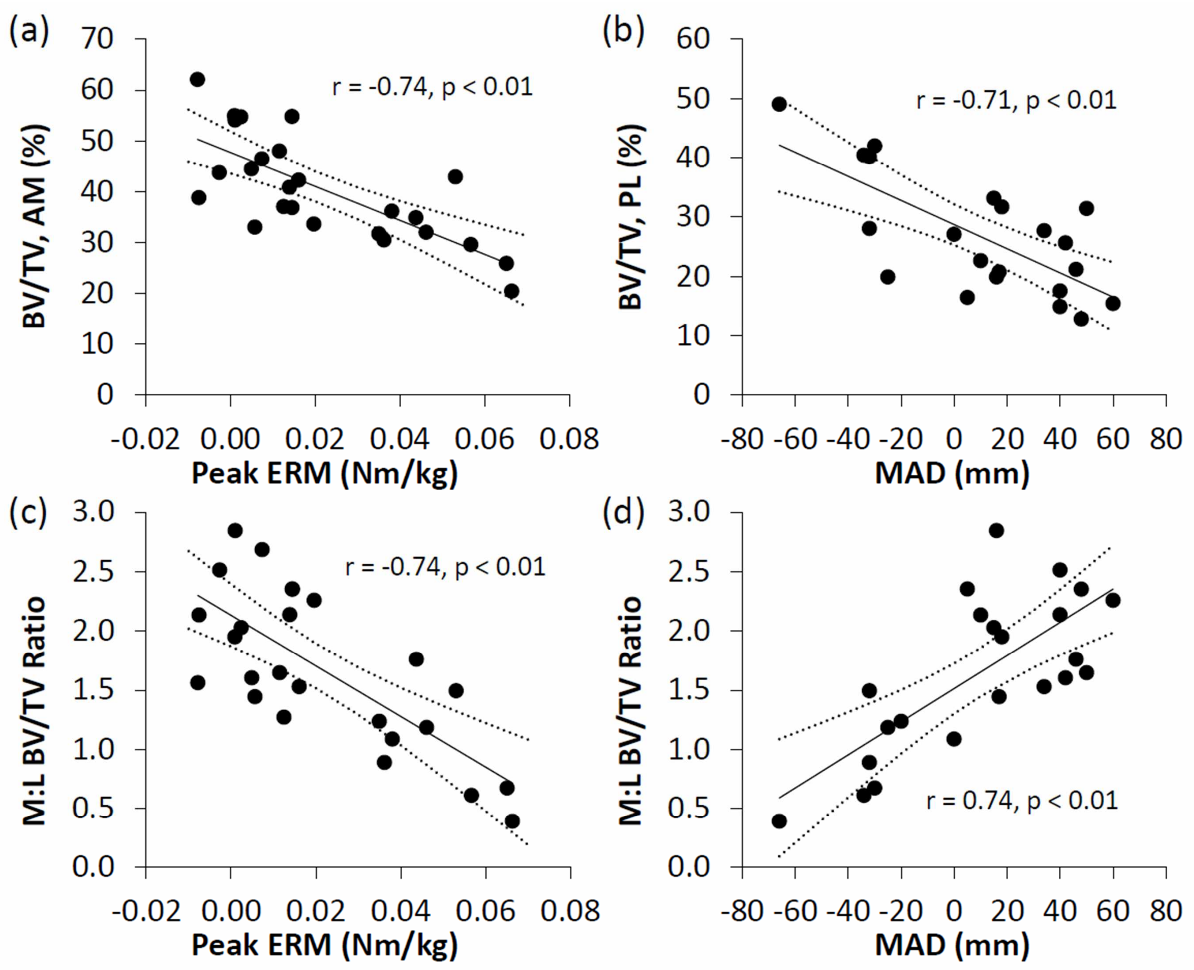

(a)
r = -0.74, p < 0.01
BV/TV, AM (%)
Peak ERM (Nm/kg)
(b)
r = -0.71, p < 0.01
BV/TV, PL (%)
MAD (mm)
(c)
r = -0.74, p < 0.01
M:L BV/TV Ratio
Peak ERM (Nm/kg)
(d)
r = 0.74, p < 0.01
M:L BV/TV Ratio
MAD (mm)